Published in final edited form as:
Biochemistry. 2011 August 9; 50(31): 6689–6700. doi:10.1021/bi200703y.

Water in the Active Site of Ketosteroid Isomerase

Philip Hanoian and **Sharon Hammes-Schiffer***
Department of Chemistry, 104 Chemistry Building, Pennsylvania State University, University Park, Pennsylvania 16802

Abstract

Classical molecular dynamics simulations were utilized to investigate the structural and dynamical properties of water in the active site of ketosteroid isomerase (KSI) to provide insight into the role of these water molecules in the enzyme-catalyzed reaction. This reaction is thought to proceed via a dienolate intermediate that is stabilized by hydrogen bonding with residues Tyr16 and Asp103. A comparative study was performed for the wild-type (WT) KSI and the Y16F, Y16S, and Y16F/Y32F/Y57F (FFF) mutants. These systems were studied with three different bound ligands: equilenin, which is an intermediate analog, and the intermediate states of two steroid substrates. Several distinct water occupation sites were identified in the active site of KSI for the WT and mutant systems. Three additional sites were identified in the Y16S mutant that were not occupied in WT KSI or the other mutants studied. The number of water molecules directly hydrogen bonded to the ligand oxygen was approximately two waters in the Y16S mutant, one water in the Y16F and FFF mutants, and intermittent hydrogen bonding of one water molecule in WT KSI. The molecular dynamics trajectories of the Y16F and FFF mutants reproduced the small conformational changes of residue 16 observed in the crystal structures of these two mutants. Quantum mechanical/molecular mechanical calculations of ^{1}H NMR chemical shifts of the protons in the active site hydrogen-bonding network suggest that the presence of water in the active site does not prevent the formation of short hydrogen bonds with far-downfield chemical shifts. The molecular dynamics simulations indicate that the active site water molecules exchange much more frequently for WT KSI and the FFF mutant than for the Y16F and Y16S mutants. This difference is most likely due to the hydrogen-bonding interaction between Tyr57 and an active site water molecule that is persistent in the Y16F and Y16S mutants but absent in the FFF mutant and significantly less probable in WT KSI.

Δ^{5}-3 Ketosteroid isomerase (KSI) is an extensively studied enzyme that serves as a useful model system for the study of the role of hydrogen bonding in enzyme catalysis. Two homologous bacterial forms of this enzyme from *Pseudomonas putida* (pKSI) and *Commamonas testosteroni* (tKSI) have been studied. In this paper, the residues are numbered according to pKSI. The structure of the active site residues in pKSI is depicted in Figure 1 (1). KSI catalyzes the stereospecific isomerization of steroid substrates such as 5-androstene-3,17-dione (5-AND) and 5,10-estrene-3,17-dione (5,10-EST) (2). In this isomerization, Asp40 serves as a general base and subsequently as a general acid in two sequential proton transfer reactions, as illustrated in Figure 2 for the 5-AND substrate. The reaction is thought to proceed via a dienolate intermediate that is stabilized by hydrogen bonding with Tyr16 and Asp103. The role of these hydrogen bonds in catalysis has been

Corresponding author: Sharon Hammes-Schiffer, Phone: 814-865-6442, Fax: 814-865-2927, shs@chem.psu.edu.

SUPPORTING INFORMATION AVAILABLE

Atom types and partial charges of each ligand used in the MD simulations, average RMSDs for each simulation with bound EQU and bound 5,10-EST, average hydrogen bond distances and angles from MD simulations, atomic isodensity surfaces from additional data sets, and superimposition of the structure of the ligand EQU from the 1OGX crystal structure and from the simulation of WT pKSI with bound EQU. This material is available free of charge via the Internet at http://pubs.acs.org.

studied extensively using site-directed mutagenesis (3–5), and the properties of these hydrogen bonds have been probed using intermediate analogs such as equilenin (EQU) in conjunction with spectroscopy and X-ray crystallography (1, 6–14). The dienolate intermediate forms of both steroid substrates and the anionic form of EQU are shown in Figure 3.

The effects of the hydrogen bond donating residues on the catalytic rate have been studied by site-directed mutagenesis using both the 5-AND and 5,10-EST substrates. The chemical steps are thought to be rate-limiting for the 5,10-EST substrate but not for the 5-AND substrate in wild-type (WT) KSI (15, 16); however, the relative effect of mutation on the catalytic rate constant (k_{cat}) is generally similar for these two substrates (17). The Y16F mutation has been found to significantly influence KSI activity, reducing k_{cat} by a factor of $10^{-3.2}$ – $10^{-4.2}$ (3, 4, 16). Mutations to less bulky residues (Y16T, Y16S, Y16A, and Y16G) were found to result in less significant reductions in k_{cat} of ~$10^{-2.3}$ (5). Each of these mutants was found to have a similar catalytic rate constant, regardless of the residue's ability to serve as a hydrogen bond donor. In the same study, crystallographic data for the Y16S mutant (PDB: 3IPT) (5) showed additional electron density in the active site not attributable to any residue. This electron density was suggested to arise from the presence of disordered water molecules in the active site. According to this interpretation, water occupies the cavity created by the Y16S mutation and plays a role in catalysis as a hydrogen bond donor during the Y16S mutant enzymatic reaction. In contrast, the Y16F mutant was proposed to prevent the formation of these additional hydrogen bonds between water and the dienolate intermediate, thus conferring an apparently enhanced energetic penalty relative to the reference reaction in water. In the Y16F mutant, the additional Y32F/Y57F mutation was found to partially restore activity, a phenomenon referred to as "pseudoreversion" (4). This triple mutant species is significantly more active than the Y16F single mutant, with a reduction in k_{cat} of ~$10^{-1.7}$ relative to WT KSI. Analysis of X-ray crystallographic data identified a small conformational change in the side chain of Y16F that was partially alleviated in the triple mutant. This conformational change was proposed to be the underlying structural cause of the pseudoreversion (4).

Several studies have provided experimental insight into the degree of solvation in the active site of KSI and its mutants. Choi and coworkers used acrylamide quenching of the fluorescence of Trp120, which hydrogen bonds to the side chain carbonyl of Asp40, to probe the solvation of the active site of apo KSI (4). They observed a greater degree of quenching in WT KSI and the Y16F/Y32F/Y57F (FFF) mutant than in the Y16F mutant. Relating these data to kinetics results, they proposed that a destabilizing structural change occurred in the Y16F mutant that was absent in WT and partially recovered by the triple phenylalanine mutation. The same study examined the effect of D_2O on the reaction rate; they observed a small effect on the catalytic rate constant in WT KSI and the FFF mutant and a significant effect on the catalytic rate constant in the Y16F mutant. Mildvan and coworkers had previously examined the WT and Y16F mutant rates in D_2O, concluding that the second step of the Y16F mutant reaction occurred only after dissociation of the intermediate (i.e., these authors proposed that this mutant followed a different mechanism) (18). Recently, Kraut et al. compared the ^{19}F NMR chemical shift of 2-fluoro-4-nitrophenolate bound to the Y16F and Y16S mutants to the solution spectra in water and THF (5). The ^{19}F chemical shift of 2-fluoro-4-nitrphenolate bound to the Y16S mutant was similar to that obtained in water, whereas the corresponding ^{19}F chemical shift in the Y16F mutant was similar to that obtained in THF. These data were interpreted to suggest that the degree of solvation in the active site was considerably greater in the Y16S mutant than in the Y16F mutant.

The role of water in protein active sites has been discussed extensively in the literature (19–22). Two previous theoretical studies have considered the presence of water in the KSI active site. Feierberg and Åqvist used empirical valence bond molecular dynamics (MD) simulations to evaluate the free energy profile of the isomerization reaction of 5-AND catalyzed by WT pKSI, both with and without a water molecule occupying a small cavity in the active site (red sphere in Figure 1) (23). Mazumder et al. performed 1.5 ns equilibrium MD simulations of the WT tKSI enzyme-substrate and enzyme-intermediate complexes of the 5-AND isomerization reaction (24). Water spontaneously entered the active site and occupied the position identified by Feierberg and Åqvist in the enzyme-substrate system but not in the enzyme-intermediate system on the timescale of their simulations. More recently, a water molecule has been observed to occupy this site in high-resolution crystal structures of the D40N/D103N mutant with bound EQU (PDB: 3FZW) (10) and the D40N mutant with bound 2-fluorophenolate (PDB: 3CPO) (25). Furthermore, the presence of a hydrogen bond between a water molecule and the nitrile group of the D40N/M116C-CN mutant has been identified using ^{13}C NMR and FTIR spectroscopies (26), supporting the presence of a water molecule within hydrogen bonding distance of the ligand oxygen.

The objective of the present paper is to identify the number of water molecules in the active site of WT pKSI and several Tyr16 pKSI mutants and to elucidate the structural and dynamical properties of these water molecules. This information is not readily obtained with experimental methods. Our goal is to explore the hypotheses previously proposed to explain the available biochemical and structural data. To address these issues, we performed MD simulations on four pKSI species: WT, Y16F, Y16S, and FFF, each with the dienolate intermediate forms of 5-AND and 5,10-EST, as well as the intermediate analog EQU. The results support the hypothesis that several water molecules occupy the active site of the Y16S mutant and form hydrogen bonds to the dienolate intermediate oxygen during the enzymatic reaction. The simulations also indicate that the FFF mutant is similar to the Y16F mutant in that both mutants accommodate similar numbers of water molecules in the active site and form similar numbers of hydrogen bonds to the dienolate oxygen. On the other hand, a qualitative difference between the Y16F and FFF mutants is the greater exchange rate observed for the active site water molecules in the FFF mutant.

METHODS

Protocol for MD simulations

We performed MD simulations of WT pKSI and the mutants Y16F, Y16S, and FFF using the program Desmond (27). Each mutant was studied with three different bound ligands: the intermediate analog EQU and the intermediate states of the steroid substrates, 5-AND and 5,10-EST, as depicted in Figure 3. In the case of EQU, the D40N mutation in the crystal structure was preserved for consistency with the experimentally studied systems. In the case of the steroid substrates, residue 40 was reverted to protonated Asp to represent the intermediate state of the enzyme-catalyzed reaction. For notational simplicity, we refer to the D40N pKSI mutant with bound EQU as WT pKSI in this paper because the oxyanion hole is not modified; the effects of this D40N mutation will be analyzed below when relevant to this study.

The initial configuration for the WT pKSI simulations was obtained from the 1OGX crystal structure (1), which corresponds to pKSI D40N with bound EQU, while the initial Y16S configuration was obtained from the 3IPT crystal structure (5), which corresponds to pKSI Y16S/D40N with bound EQU. We did not initiate the Y16F simulations from the 1OHO crystal structure (28), which corresponds to pKSI Y16F/D40N with bound EQU, because the EQU in this structure is bound in an alternative conformation where the D-ring carbonyl group is hydrogen bonded to Asp103. Instead, the Y16F and FFF mutants were modeled

from the 1OGX crystal structure, with phenolic oxygens removed from the relevant tyrosine residues. This procedure is reasonable because the Y16F and FFF mutations are characterized by small local conformational changes rather than large-scale structural rearrangements of the protein (4).

In each case, KSI was simulated as a dimer, with both active sites containing the same mutations and occupied by the same ligand. The missing N and C-terminal residues (1-3 and 127-130) were modeled from the 3FZW crystal structure (10) by minimization of the backbone root mean square deviation (RMSD) with respect to the five subsequent and preceding residues, respectively. Since residue 131 is unresolved in all structures, it was modeled with the utility Profix (29), as were the unresolved polyglycine residues at positions 62–64 in structure 3IPT. To dock the 5-AND and 5,10-EST steroids into the active site, the HF/6-31G* geometry-optimized steroid structure was superimposed onto the EQU by minimizing the RMSD between the steroid atoms C3, O3, C4, C17, and O17 and the corresponding atoms in EQU. Additionally, for the simulations with the 5-AND and 5,10-EST ligands, the D40N amide nitrogen was converted to oxygen and protonated *in silico* to represent the intermediate state of the enzymatic reaction. The protonation states of the titratable residues were determined using H^{++} (30) and by inspection of hydrogen bonding interactions in the crystal structures.

The dimer was solvated in an orthorhombic box of TIP3P (31) water molecules extending at least 10 Å beyond the enzyme, and ten sodium ions were added to maintain charge neutrality using the Desmond system builder implemented in Maestro (32). We used the AMBER99SB (33, 34) force field to model the protein. For each ligand, we determined restrained electrostatic potential (RESP) (35) partial atomic charges at the HF/6-31G* level of theory using Gaussian 03 (36) and the AMBER (37) RESP binary. The missing force field parameters were obtained from the Generalized Amber Force Field (38). The atom types and partial charges used for each ligand are provided in Table S1. We used a time step of 1 fs, a 12 Å non-bonded cutoff, and the smooth particle mesh Ewald method (39) for long-range electrostatics.

For each system, we followed an extensive equilibration procedure prior to data collection. First all modeled residues were geometry optimized, followed by optimization of the water and ions, and finally optimization of the full system. Next the water and ions were subjected to 500 ps of equilibration at constant NVT (i.e., a canonical ensemble) using the Nosé-Hoover (40, 41) thermostat at 300 K. The full system was then gradually heated to 300 K in increments of 50 K, holding the temperature constant at each interval for 50 ps using the Martyna-Tobias-Klein NPT algorithm (42) at a pressure of 1 atm and changing the temperature after each interval over 10 ps. The full system was then equilibrated at 300 K for 500 ps at constant NPT and subsequently for 500 ps at constant NVT. Following equilibration, 20 ns of data were collected at constant NVT with configurations saved every 1 ps. We propagated two independent trajectories for each different system (i.e., for each mutant with each bound ligand). Since each system contains a KSI homodimer, each independent trajectory yielded two data sets. The average backbone RMSDs of the well-folded residues (2-127) with respect to the average structure were below 1 Å for all trajectories, indicating that this equilibration procedure is sufficient (Tables S2 and S3). Additionally, as depicted in Figure 4, the root mean squared fluctuations of the C_α atoms of these residues from the WT and Y16S simulations with bound EQU agree well with those calculated from the X-ray crystallographic B-factors (43, 44) of the 1OGX and 3IPT crystal structures, respectively.

For each system, we determined the radial distribution function, $g(r)$, between the ligand oxygen and water oxygens. Running coordination numbers of water oxygens about the ligand oxygen, $n(r)$, were calculated according to the following expression (45):

$$n(r)=4\pi\rho\int_0^r g(r')r'^2dr' \quad (1)$$

where ρ is the number density of water in the system. In addition, to determine the average locations of bound water molecules in three dimensions, we calculated atomic isodensity surfaces for all water molecules within a cube with sides of length 14 Å centered at the ligand oxygen (46). For this purpose, configurations were aligned to a laboratory frame by placing the steroid O3 at the origin, C3 along the x-axis, and C4 in the x-y plane; the same alignment procedure was performed using the corresponding atoms in EQU (O1, C1, and C2, respectively). Atomic positions were binned using a three-dimensional grid with cubic sides of length 0.25 Å. The population of each bin was then normalized by dividing by the number of configurations, the volume element of numerical integration, and the water density of the periodic simulation box, resulting in a unitless quantity.

MD simulations using classical force fields are associated with several limitations. The use of a fixed atomic point charge representation of the highly interconnected hydrogen bond network in the KSI active site constitutes a limitation on the quantitative accuracy of the representation of these oxyanion hole residues. In addition, the TIP3P water model used in this study is just one of a vast number of available water models (47), and quantitative but probably not qualitative differences may be observed with other water models. Furthermore, as bonds cannot break or form using these force fields, the classical MD simulations presented here cannot be used to evaluate the free energy barriers of the reaction and calculate the catalytic rate constants. The empirical valence bond MD approach that has been applied to KSI by Warshel (48, 49), Åqvist (23, 48), and in our own group (50, 51) can be used to evaluate these rate constants, although this procedure requires parameterization of the empirical valence bond potential. Due to the long simulation times that have been required to obtain statistically meaningful configurations of each system with water occupying the active site, the present approach is a precursor to such more advanced treatments of these systems.

Solvent exclusion properties of ligands

All of our MD simulations were performed with a bound ligand, which in some cases may prevent water from entering the active site. In particular, water did not enter the active site often in trajectories with bound 5-AND but did enter freely in trajectories with EQU and in the majority of trajectories with 5,10-EST. In the enzymatic reaction, however, water is able to enter the active site prior to substrate binding. The lack of water entering the active site during the MD trajectories with certain ligands is not biologically significant but rather is the result of preparing the system without water initially in the active site. In this subsection, we analyze the differences among the three ligands with respect to the entry of water into the active sites.

Although the magnitude of the partial negative charge on the ligand oxygen is similar for EQU and the intermediate state of the steroid substrates, as illustrated by the RESP charges in Table S1, the steroid substrate 5-AND has a qualitatively different topology from EQU in the A and B rings. As a result, in contrast to the simulations with bound EQU, water was nearly always excluded from the KSI active site in the simulations with bound 5-AND. Water was observed to enter the active site in only three data sets with bound 5-AND, namely one active site in one of the two independent trajectories propagated for the WT,

Y16F, and Y16S systems. In each of these systems, only one water molecule entered the active site during the entire 20 ns trajectory. An additional independent trajectory was performed in each case for which water was observed to enter the active site, and no water entered either active site in these additional three trajectories. Thus, a water molecule was observed to enter the active site in only three out of the 22 total data sets generated with bound 5-AND. The low probability of water exchange observed in these simulations is consistent with the results obtained by Mazumder et al., where water exchange was not observed in 1.5 ns simulations with the same ligand (24). These observations indicate that the statistically meaningful observation of water entry into the active site for bound 5-AND would require substantially longer MD trajectories and enhanced sampling methods. As a result, we do not provide an analysis of the simulations with the bound 5-AND substrate.

The low degree of water entry into the active sites for the simulations with bound 5-AND is most likely due to the C19 methyl group, which inhibits water entry into the active site. In this case, the alternative steroid substrate, 5,10-EST, which does not bear a C19 methyl group, would be expected to behave more similarly to EQU than to 5-AND. The results obtained from trajectories with bound 5,10-EST were less uniform than those with bound EQU, but water entered the active site in the majority of the 5,10-EST trajectories. In one trajectory for the Y16S mutant, the ligand in one of the active sites was observed to partially unbind, which was not observed in either active site of a third independent trajectory. In the FFF mutant, no water was observed to enter one of the two KSI active sites in each of three independent trajectories. One possible interpretation of these results is that the FFF mutation has reduced the affinity of water for the active site. Based on the similarity of the remaining data sets to those obtained with bound EQU, however, a more plausible interpretation is that the absence of water in the active site for these trajectories indicates insufficient sampling. For the analysis below, these data sets have been omitted, although we observed no significant increase in the RMSD of the C_α or side-chain heavy atoms for these monomers that would indicate a loss of stability in the protein fold. For the remainder of the paper, our analysis of the systems with bound 5,10-EST focuses on the trajectories for which water entered the active site during equilibration, indicating sufficient sampling to examine the structure and dynamics of water in these active sites.

QM/MM calculations

To further analyze the configurations obtained from the MD simulations, we performed quantum mechanical/molecular mechanical (QM/MM) geometry optimizations using the program QSite (52) for a subset of the configurations from the MD simulations. These calculations provide a connection to the experimentally measured NMR chemical shifts (7, 53). For each system with bound EQU, configurations were extracted from the first MD trajectory at intervals of 1 ns. The residues Y16(F/S), Y32(F), D40N, Y57(F), D103, and EQU in the active site of chain A were represented quantum mechanically at the DFT B3LYP/6-31G** level of theory using frozen orbitals for the boundaries. In each configuration, any water molecule within 5.5 Å of the ligand oxygen was also represented quantum mechanically. The remainder of the protein was represented by the OPLS2005 MM force field (54). Only the atoms in the QM region were geometry optimized, with all other atoms remaining fixed. Following geometry optimization, the isotropic shieldings of the QM atoms were calculated at the DFT B3LYP level of theory using gauge-including atomic orbitals (55) and the cc-pVTZ basis set (56), with hydrogen caps between C_α and C_β. The NMR chemical shift was then calculated as the difference between the shielding of tetramethylsilane at the same level of theory in the gas phase and the shielding of the nucleus of interest.

RESULTS AND DISCUSSION

The objective of this work is to examine the structure and dynamics of water in the active sites of WT pKSI and a series of Tyr16 mutants. First we present the analysis of the MD simulations performed with the intermediate analog EQU, identifying the locations of the active site water molecules and quantifying the numbers of hydrogen bonds formed with the EQU oxygen. Subsequently, we compare the results obtained with bound EQU to those obtained with the bound steroid intermediates 5-AND and 5,10-EST, focusing on differences in the molecular topologies of these ligands. We then examine the differences between the active site conformations of the Y16F and FFF mutants in more detail, comparing the computational results to published structural data. In the absence of significant structural differences between these two mutants, we examine the fluctuations of water in the active site, identifying qualitative differences in the behavior for WT pKSI and the mutants. We conclude with the presentation of calculated ^{1}H NMR chemical shifts for the protons in the pKSI hydrogen-bonding network with bound EQU, where far-downfield chemical shifts are observed in the presence of water molecules in the active site.

Simulations with Bound Equilenin

In simulations with bound EQU, water was observed to enter the KSI active sites without disturbing the hydrogen bonding of the ligand to the oxyanion hole residues. The radial distribution functions $g(r)$ between the ligand oxygen and water oxygens for trajectories with bound EQU are depicted in Figure 5A, and the running coordination numbers $n(r)$ of water oxygens about the ligand oxygen are depicted in Figure 5C. The distribution functions have several well-defined peaks, with the first maximum corresponding to a direct ~2.8 Å hydrogen-bonding distance to the ligand oxygen. The second maximum corresponds to a second-shell hydrogen-bonding interaction and is shifted to slightly shorter distances for Y16S than for the other species, suggesting that a different hydration arrangement occurs in the Y16S mutant. The first minimum of $g(r)$ is located at ~3.5 Å. As determined by the running coordination number at this distance, ~2 waters reside within direct hydrogen-bonding distance of the EQU oxygen in the Y16S mutant, while ~1 water is within direct hydrogen-bonding distance in the Y16F and FFF mutants. In WT pKSI, one water was intermittently hydrogen bonded to the EQU oxygen, resulting in a coordination number of ~0.4 at this distance.

To identify the locations of the water occupation sites in these trajectories, we calculated atomic isodensity surfaces of water in the KSI active site. The results are shown in Figure 6 for a representative data set, with the average structure of the active site heavy atoms included. (Residue D40N has been omitted for clarity.) The isodensity surfaces for the remaining three data sets are provided in Supporting Information Figure S1 for comparison. We observed four water occupation sites in all EQU trajectories (numbered 1–4 in Figure 6A), with three additional sites (numbered 5–7 in Figure 6E) observed in the Y16S mutant. As suggested by the radial pair distribution function data, only one discrete site (site 1) was observed within hydrogen bonding distance of the ligand oxygen in the WT, Y16F, and FFF trajectories. This site corresponds to the occupation site that has been observed in previous MD simulations of WT KSI (23, 24) and in recent high-resolution crystal structures (10, 25). The water molecule occupying this site is capable of hydrogen bonding to Tyr57, the ligand oxygen, and Asp40Asn. In the Y16F mutant, Tyr57 usually formed hydrogen bonds with Tyr32 and the water molecule in site 1, whereas in WT pKSI, Tyr57 usually formed hydrogen bonds with Tyr16 and Tyr32 (Figure 1), with less frequent hydrogen bonding to the water molecule in site 1. These hydrogen bonding interactions will be quantified and discussed in more detail below.

We also observed several water occupation sites in the KSI active site that are distal to the oxyanion hole. These distal water occupation sites are observed independently of the oxyanion hole mutation but are dependent on the topology of the bound ligand. Site 2 lies above the A ring of EQU, with the proton directed toward the partial negative charge of the conjugated π system. This region corresponds to the same location as the C19 methyl group of 5-AND. Thus, this water is expected to be sterically excluded by the bound 5-AND ligand and will be discussed in more detail below. Site 3 lies above site 2, forming a hydrogen-bonded network of water that is in contact with the bulk solvent. This site is separated from the oxyanion hole residues by the aromatic rings of Phe56 and Tyr57. In the simulations, Phe56 is shifted by ~1 Å relative to the 1OGX crystal structure, providing additional space to accommodate the water molecules in sites 2 and 3, as shown in Figure 7A. The conformational changes observed relative to the available crystal structures will be discussed in more detail below. Site 4 interacts with the side chain carbonyl group of D40N and is also in contact with the bulk solvent.

We identified three additional water occupation sites within the Y16S mutant pKSI active site that were not present in the other systems. Sites 5 and 6 are directly hydrogen bonded to the ligand, while site 7 is buried more deeply within the cavity and hydrogen bonded to the other two water molecules. Although three sites within direct hydrogen bonding distance of the ligand oxygen (sites 1, 5, and 6) are observed for Y16S, all three sites are rarely occupied concurrently. As a result, three sites within direct hydrogen bonding distance of the ligand oxygen were resolved, but the running coordination number of the ligand oxygen for the Y16S mutant is only ~2 at this distance. Furthermore, in several data sets, sites 1 and 5 partially overlap, forming a continuous band of oxygen density rather than discrete sites, as illustrated in Figure S1B.

The hydroxyl group of Y16S was not observed to donate a hydrogen bond to the bound EQU and instead forms a hydrogen bond with the backbone carbonyl group of Leu12 during most of the trajectories, with occasional excursions to hydrogen bond to Met13 or to a water molecule. This side chain conformation is slightly different from that observed in the 3IPT crystal structure (i.e., the initial configuration of the system), where the Y16S hydroxyl was observed to hydrogen bond to the backbone carbonyl group of Met13. Both of these carbonyl groups are located on the same face of the A1 α-helix, with the Y16S side chain situated between them, and the observed conformational change corresponds to a rotation of this side chain about its C_α–C_β bond. As noted by Kraut et al., the absence of direct hydrogen bonding interactions between the Y16S side chain and the ligand oxygen is consistent with the negligible differences among the catalytic rate constants of the Y16T, Y16S, Y16A, and Y16G mutants, where Thr and Ser have the capability of forming hydrogen bonds but Ala and Gly do not have this capability (5).

The results obtained for the Y16S mutant are consistent with the proposal from biochemical studies and X-ray crystallography that two to three water molecules occupy the Y16S mutant active site cavity and form hydrogen bonds with the steroid during the enzymatic reaction. The ^{19}F NMR experiments performed by Kraut et al. probed the local solvation environment of the Y16F and Y16S oxyanion holes directly using a bound fluorophenol (5). They found the local environment of the ^{19}F nucleus to be different in the two mutants, with the Y16S mutant appearing to possess a more polar solvation environment than the Y16F mutant. The presence of the additional water molecules occupying sites 5 – 7 in the MD trajectories of the Y16S mutant constitutes a significant enhancement of the solvation of the active site and is consistent with the differences between the Y16F and Y16S mutants identified by the ^{19}F NMR experiments.

To investigate whether the reduction in the catalytic rate constant associated with each mutant can be explained by differences in hydrogen bonding, we determined the average number of hydrogen bonds to the ligand oxygen for each species. For this purpose, a hydrogen bond was defined to have an O–O distance less than 3.5 Å and an O–H–O angle within 30° of linearity. The results of this analysis are provided in Table 1. The average number of hydrogen bonds in each species is qualitatively similar, with the Y16F and FFF mutants exhibiting slightly less hydrogen bonding to the ligand and the Y16S mutant exhibiting slightly more hydrogen bonding to the ligand relative to WT pKSI. The contributions from each hydrogen-bonding residue are provided in Table 2 as the percentage of configurations containing an intact hydrogen bond to the ligand oxygen from each donor. In the case of hydrogen bonds with water, configurations were distinguished based on the total number of hydrogen bonds to water, which was observed to range from one to three. The results of this decomposition show that the Asp103 hydrogen bond remains predominantly intact, while the absence of a Tyr16 hydrogen bond is compensated by additional hydrogen bonds to water, resulting in similar numbers of hydrogen bonds in each species. The presence of a hydrogen bond between the site 1 water and EQU is consistent with a recent ^{13}C NMR and FTIR study that suggested a hydrogen bond between an active site water molecule and the nearby nitrile group of the D40N/M116C-CN mutant (26).

The thermally averaged structures obtained from the MD trajectories of each mutant were compared to the relevant crystal structures by aligning the C_α atoms of residues 2-127 in each monomer. As shown in Figure 7A, the overall structure of the D40N-EQU active site was well-maintained, although small conformational changes occurred in the side chain of F56 and the EQU ligand in the simulation. These conformational changes create a larger cavity in the active site that is expected to facilitate water exchange. The conformational change in EQU was not due to significant differences in the structure of the EQU ligand itself, as shown in Figure S3, but rather to differences in its binding position in the active site. These conformational changes were observed in all simulations with bound EQU. This discrepancy may arise from limitations of the molecular mechanical force field or from active site water molecules that are present in the simulations but not in the crystal structures.

Simulations with Bound Steroid Intermediates

As discussed above, the simulations with bound 5-AND did not allow a significant degree of water entry into the oxyanion hole on the timescale of these trajectories. In the simulations with bound EQU, water gained access to the oxyanion hole via site 2; thus, solvent exclusion from this site would be expected to preclude water entry into the oxyanion hole itself. The C19 methyl group that is present in 5-AND but absent in EQU is a significant factor in the differing levels of water entry for bound EQU and 5-AND. Indeed, superimposition of 5-AND onto EQU in the presence of the atomic isodensity surfaces obtained with bound EQU indicates that the C19 methyl group of 5-AND sterically clashes with the water site 2, as illustrated in Figure 8.

The alternative steroid substrate, 5,10-EST, does not bear a C19 methyl group and therefore behaves more similarly to EQU than to 5-AND with respect to solvent exclusion properties. The radial distribution functions and running coordination numbers from trajectories with bound 5,10-EST are depicted in Figures 5B and 5D, respectively. The population of water in the KSI active site for trajectories with bound 5,10-EST is decreased relative to that observed for trajectories with bound EQU, but the locations of the peaks and the relative populations among mutants are qualitatively similar to the results obtained with bound EQU.

The atomic isodensity surfaces illustrating the water occupation sites in the simulations with bound 5,10-EST are depicted in Figures 6B, 6D, 6F, and 6H for a representative data set,

with the corresponding figures for additional data sets provided in Figure S2. When water was observed to enter the active site, only the sites that were occupied in the trajectories with bound EQU were populated. Although water occupation of site 2 is observed both with bound EQU and with bound 5,10-EST, the location of this site is shifted toward the B ring with bound 5,10-EST, and the proton interacts with the partial negative charges on C5 and C10. The only site observed with bound EQU that is generally absent from the trajectories with bound 5,10-EST is site 4, which interacts with the carbonyl of D40N in simulations with bound EQU. (A small amount of density is observed in this site in Figure 6H, but this density is not statistically significant.) This observation suggests that the additional hydrogen atoms on the B ring of 5,10-EST enhance the solvent exclusion properties of the bound steroid relative to EQU. Alternatively, the presence of the D40N mutation in the EQU simulations may enhance the occupancy of water in the active site, relative to the protonated Asp40 side chain in the 5,10-EST simulations. The similarity of the sites identified from the atomic isodensity surfaces in the oxyanion hole (i.e., sites 1, 5, 6, and 7) for bound EQU and 5,10-EST, however, suggests that the water occupation of these sites is likely to be consistent, although occupation of the distal sites depends on ligand topology. Thus, EQU serves as a useful analog for identification of these sites via MD simulation.

Comparison of active site conformations in Y16F and FFF mutants

Although the catalytic rate constants for the Y16F and FFF mutants differ significantly, our MD simulations indicate that the hydrogen bonding characteristics of the bound ligand are similar for these two mutants. Table 1 indicates that the average number of hydrogen bonds involving the ligand oxygen is similar for the Y16F and FFF mutants with either EQU or 5,10-EST bound to the active site. The more detailed analysis of hydrogen bonding provided in Table 2 also indicates that these two mutants behave similarly. These tables imply that the number of hydrogen bonds and the identities of the hydrogen bond donors are similar for the two mutants. Furthermore, the average hydrogen bonding distances and angles from the MD simulations, provided in Tables S4 and S5, respectively, are also similar for the Y16F and FFF mutants. When a subset of configurations were subsequently optimized at the QM/MM level, the Asp103-EQU hydrogen bond was observed to be slightly shorter in the FFF mutant than in the Y16F mutant, as shown in Table 3, but this difference is not statistically meaningful.

Based on the average structures from the MD simulations, we observed a small conformational change in the side chain of residue 16 for both the Y16F and FFF mutants relative to WT pKSI, as illustrated in Figures 7B and 7C, respectively. These conformational changes are in agreement with the conformational changes observed by Choi and coworkers in the crystal structure of the Y16F mutant with bound EQU (PDB: 1OHO) (28) and in the FFF apo crystal structure (PDB: 1E97) (4). Although the EQU in the 1OHO structure is bound with its D-ring carbonyl group in the oxyanion hole, a similar and more pronounced conformational change in the side chain of residue 16 was also observed in the apo crystal structure of the Y16F mutant (PDB: 1EA2) (4). Note that the initial structures for our MD trajectories of the Y16F and FFF mutants were obtained from the 1OGX structure with the tyrosines modified to phenylalanine *in silico*. Thus, the reproduction of the Tyr16 conformational change in the MD trajectories provides a degree of validation of the MM force field. Furthermore, the conformational changes in the side chain of residue 16 observed in the Y16F and FFF mutant trajectories are very similar, as shown in Figure 7D. These conformational changes may arise from similar interactions of the mutated residue 16 with the bound water molecules in the oxyanion hole. The next subsection will illustrate that the fluctuations of the water molecules in the active site are different for the Y16F and FFF mutants.

Fluctuations of Water in the Active Site

For trajectories in which water occupied the active site, the water typically entered the active site during the equilibration phase. Once a water molecule entered the active site, however, it did not remain there throughout the trajectory. Instead, the water molecules in the active site were observed to exchange on timescales that were dependent on the simulated species. These results are consistent with the differences observed in previous MD simulations of the reactant and intermediate states of 5-AND (24). Although the water exchange events did not occur frequently enough to calculate a statistically meaningful time correlation function or exchange rate, a qualitative analysis provides insights into differences among the species.

To qualitatively illustrate the rate of exchange, we monitored the identity of the water molecules within 3.5 Å of the ligand oxygen as a function of time. The results of this analysis are depicted in Figure 9 for a representative data set. In WT pKSI, the bound water molecules in the oxyanion hole exchanged many times over the course of the 20 ns simulation, with residency times of ~1 ns or less. In contrast, the water molecules in the oxyanion hole of the Y16F and Y16S mutants were observed to remain in the active site for longer periods, although additional water molecules exchanged on shorter timescales as well. Specifically, for both the Y16F and Y16S mutants with bound EQU, a single water molecule remained hydrogen bonded to the ligand oxygen during almost the entire 20 ns trajectory. For the Y16S mutant, a second water molecule also remained bound to the ligand oxygen for more than 10 ns. Qualitatively similar behavior was observed for these mutants with bound 5,10-EST, although one or two exchanges of the stably hydrogen-bonded water molecules were observed during the 20 ns trajectory. In the FFF mutant, water molecules were observed to exchange less frequently than in WT pKSI but significantly more frequently than in the Y16F and Y16S mutants.

To further investigate these observations, we examined the hydrogen-bonding interactions between Tyr57 and the water molecules in the active site with bound EQU. In the FFF mutant, Tyr57 is mutated to Phe and thus cannot hydrogen bond to these water molecules. In WT pKSI, Tyr57 is able to hydrogen bond to Tyr16 (Figure 1) and is therefore less likely to hydrogen bond to a water molecule. Comparison of the Y16F mutant to WT pKSI indicates a pronounced difference in the percentage of configurations with intact hydrogen bonds between Tyr57 and water in site 1. In WT pKSI, Tyr57 serves as a hydrogen bond donor to a water molecule (i.e., directs its hydroxyl group toward the partial negative charge on the water oxygen) in 4% of the configurations and serves as a hydrogen bond acceptor from a water molecule in 11% of the configurations. In contrast, in the Y16F mutant, Tyr57 serves as a hydrogen bond donor to a water molecule in 79% of the configurations and as a hydrogen bond acceptor in 3% of the configurations. The Y16S mutant behaves similarly to the Y16F mutant in this respect. These quantities varied among the independent trajectories by 5% or less in all cases. This analysis of the hydrogen bonding between Tyr57 and active site water molecules provides a plausible explanation as to why the exchange rate for water molecules in the active site is greater for WT pKSI and the FFF mutant than for the Y16F and Y16S mutants. The difference between the fluctuations of the water molecules in the FFF mutant and the Y16F mutant may be related to the difference in catalytic rate constants observed for these two mutants. This possible connection will be explored in future calculations of the free energy barriers using an empirical valence bond potential.

^{1}H NMR Chemical Shifts

To provide a direct connection to experimental data, we performed QM/MM geometry optimizations and NMR chemical shift calculations to determine whether the presence of water in the KSI active site is consistent with the formation of short hydrogen bonds in the KSI active site and their associated far-downfield (> 14 ppm) ^{1}H NMR chemical shifts. In

our previous study of a series of substituted phenolates (53), the calculated chemical shift of the most downfield ^{1}H NMR resonance was found to be ~4 ppm further downfield than the corresponding experimental value, although the trends as a function of phenolate pK_a were well reproduced. We hypothesized that sampling configurational space would improve the quantitative agreement in these calculations. Here, we present NMR chemical shifts for each system with bound EQU calculated as an average of 21 individually optimized configurations sampled every 1 ns from the MD trajectories.

The calculated ^{1}H NMR chemical shifts are presented in Table 4. For WT pKSI, we observe two far-downfield NMR chemical shifts that are in reasonable agreement with the corresponding experimental spectra (6). In Ref. (6), two far-downfield NMR chemical shifts were resolved for pKSI with bound EQU at 16.8 and 13.1 ppm. Our two most downfield chemical shifts may correspond to these two peaks. Alternatively, the hydrogen-bonded protons of Tyr16 and Tyr57 may correspond to these two experimentally resolved shifts, while the Asp103 hydrogen-bonded proton may correspond to an unresolved peak in the middle. The observation of far-downfield ^{1}H NMR chemical shifts arising from short active site hydrogen bonds illustrates that the presence of water in the KSI active site does not preclude these physical phenomena.

Although the relative ordering of the chemical shifts of Tyr16, Asp103, and Tyr57 remains consistent, the quantitative values obtained from the present calculations are significantly improved relative to the previous values calculated for phenols (53), with errors of ~1–2 ppm persisting. According to the calculations, the chemical shift of the Asp103 hydrogen bonded proton increases by ~1.5 ppm in the Y16F mutant relative to WT pKSI. The presence of a far-downfield resonance in the Y16F mutant is consistent with the more recent spectrum acquired for this mutant of tKSI, where a single far-downfield resonance was observed at 17.4 ppm (5). The significant increase in the chemical shift of the Asp103 hydrogen-bonded proton in response to the Y16F mutation is consistent with the observed coupling of the Tyr16 and Asp103 hydrogen bonds (10, 53). To our knowledge, no ^{1}H NMR spectra have been published for the Y16S or FFF systems. In each of these cases, as in the Y16F system, the calculations predict the presence of one far-downfield resonance corresponding to the Asp103 hydrogen-bonded proton. The Tyr32 hydrogen-bonded proton in all species and the Tyr57 hydrogen-bonded proton in the mutants are calculated to have chemical shifts <10 ppm, which could not be distinguished from the other peaks in the complicated spectrum of the protein.

The hydrogen-bonding distances of Asp103 and Tyr16 to the EQU oxygen provide insight into the ^{1}H NMR chemical shifts because of the correlation between hydrogen-bonding distances and chemical shifts (57). The average hydrogen-bonding distances calculated with QM/MM methods are provided in Table 3. The calculated Asp103-EQU hydrogen-bonding distance of 2.57 Å for the Y16S mutant agrees well with the distance of 2.57 Å observed in the 3IPT crystal structure for the D40N/Y16S mutant with bound EQU (5). Based on this relatively short distance, this hydrogen-bonded proton is expected to correspond to a far-downfield NMR chemical shift (57). The calculated Tyr16-EQU and Asp103-EQU hydrogen-bonding distances of 2.52 Å and 2.62 Å, respectively, for WT pKSI do not agree as well with the values of 2.67 Å and 2.55 Å from the 1OGX crystal structure of the D40N mutant with bound EQU (6), although these calculated distances do agree well with the values of 2.48 Å and 2.61 Å from the more recent 2PZV crystal structure of the D40N mutant with bound phenolate (7). The far-downfield NMR chemical shifts observed for the D40N mutant with bound EQU are also similar to those observed with bound phenolate (6, 7).

CONCLUSIONS

In this paper, we presented MD calculations that provide insight into the structural and dynamical properties of water in the ligand-bound KSI active site for the WT and mutant KSI systems. The atomic isodensity surfaces of water obtained from the MD trajectories were used to identify water occupation sites in the active site of the enzyme. We identified three additional sites in the Y16S mutant that are not occupied in WT pKSI or the other mutants studied. These results support the hypothesis from biochemical studies of the Y16S mutant that two to three water molecules occupy the oxyanion hole and hydrogen bond to the steroid substrate during catalysis in this mutant. We also used QM/MM methods to calculate the ^{1}H NMR chemical shifts of the protons in the hydrogen-bonding network for configurations obtained from the MD trajectories. The results of these calculations are in reasonable agreement with the available experimental data and suggest that the presence of water in the active site does not prevent the formation of short hydrogen bonds with far-downfield chemical shifts. Furthermore, we observed fluctuations in the occupation of these sites with water exchange rates on the picosecond to nanosecond timescale, which is consistent with the observation of disordered density in the crystal structure of the Y16S mutant.

Our MD simulations also enabled a comparison of water in the active site of the Y16F and FFF mutants. Our analysis suggests that a water molecule occupies a site in the oxyanion hole and hydrogen bonds to the ligand oxygen for both the Y16F and FFF mutants. Moreover, the calculations indicate that the number of water molecules in the active site, the positions of these water molecules, and the number of hydrogen bonds to the ligand oxygen are similar for the Y16F and FFF mutants. Comparison of the average structures from the MD trajectories to crystal structures of these mutants illustrates that the MD trajectories reproduced the small conformational change of residue 16 associated with these two mutants. This conformational change may be due to interactions between Phe16 and the water molecule hydrogen-bonded to the ligand oxygen. In addition, our analysis indicated that the active site water molecules exchange much more frequently for WT pKSI and the FFF mutant than for the Y16F and Y16S mutants. This distinction is most likely due to the hydrogen-bonding interaction between Tyr57 and water that is persistent in the Y16F and Y16S mutants but absent in the FFF mutant and significantly less probable in WT pKSI. This qualitative difference between the Y16F and FFF mutants could potentially be related to the experimentally measured difference in the catalytic rate constants of these two mutants. Future simulations of the chemical reactions using empirical valence bond MD methods could provide further insight into these issues.

Supplementary Material

Refer to Web version on PubMed Central for supplementary material.

Acknowledgments

We thank Alexander Soudackov, Paul Sigala, Jason Schwans, and Dan Herschlag for helpful discussions.

Funding acknowledgment: This work was funded by NIH Grant No. GM56207.

Abbreviations

KSI	Δ^{5}-3-ketosteroid isomerase
pKSI	KSI from *Pseudomonas putida*

tKSI	KSI from *Commamonas testosteroni*
QM/MM	quantum mechanical/molecular mechanical
MD	molecular dynamics
WT	wild-type
FFF	Y16F/Y32F/Y57F
EQU	equilenin
5-AND	5-androstene-3,17-dione
5	10-EST, 5,10-estrene-3,17-dione
RMSD	root mean squared deviation
RESP	restrained electrostatic potential

References

1. Ha NC, Kim MS, Lee W, Choi KY, Oh BH. Detection of large pKa perturbations of an inhibitor and a catalytic group at an enzyme active site, a mechanistic basis for catalytic power of many enzymes. J Biol Chem. 2000; 275:41100–41106. [PubMed: 11007792]
2. Pollack RM. Enzymatic mechanisms for catalysis of enolization: ketosteroid isomerase. Bioorg Chem. 2004; 32:341–353. [PubMed: 15381400]
3. Jang DS, Cha HJ, Cha SS, Hong BH, Ha NC, Lee JY, Oh BH, Lee HS, Choi KY. Structural double-mutant cycle analysis of a hydrogen bond network in ketosteroid isomerase from *Pseudomonas putida* biotype B. Biochem J. 2004; 382:967–973. [PubMed: 15228388]
4. Choi G, Ha N-C, Kim M-S, Hong B-H, Oh B-H, Choi KY. Pseudoreversion of the catalytic activity of Y14F by the additional substitution(s) of tyrosine with phenylalanine in the hydrogen bond network of Delta-5-3-ketosteroid isomerase from Pseudomonas putida biotype B. Biochemistry. 2001; 40:6828–6835. [PubMed: 11389596]
5. Kraut DA, Sigala PA, Fenn TD, Herschlag D. Dissecting the paradoxical effects of hydrogen bond mutations in the ketosteroid isomerase oxyanion hole. Proc Natl Acad Sci USA. 2010; 107:1960–1965. [PubMed: 20080683]
6. Cho HS, Ha NC, Choi G, Kim HJ, Lee D, Oh KS, Kim KS, Lee W, Choi KY, Oh BH. Crystal structure of Δ^5-3-ketosteroid isomerase from *Pseudomonas testosteroni* in complex with equilenin settles the correct hydrogen bonding scheme for transition state stabilization. J Biol Chem. 1999; 274:32863–32868. [PubMed: 10551849]
7. Kraut DA, Sigala PA, Pybus B, Liu CW, Ringe D, Petsko GA, Herschlag D. Testing electrostatic complementarity in enzymatic catalysis: Hydrogen bonding in the ketosteroid isomerase oxyanion hole. PLoS Biology. 2006; 4:501–519.
8. Petrounia IP, Blotny G, Pollack RM. Binding of 2-naphthols to D38E mutants of 3-oxo-Δ^5-steroid isomerase: Variation of ligand ionization state with the nature of the electrophilic component. Biochemistry. 2000; 39:110–116. [PubMed: 10625485]
9. Petrounia IP, Pollack RM. Substituent effects on the binding of phenols to the D38N mutant of 3-oxo-Δ^5-steroid isomerase: A probe for the nature of hydrogen bonding to the intermediate. Biochemistry. 1998; 37:700–705. [PubMed: 9425094]
10. Sigala PA, Caaveiro JMM, Ringe D, Petsko GA, Herschlag D. Hydrogen bond coupling in the ketosteroid isomerase active site. Biochemistry. 2009; 48:6932–6939. [PubMed: 19469568]
11. Zeng B, Bounds PL, Steiner RF, Pollack RM. Nature of the Intermediate in the 3-Oxo-Δ^5-steroid Isomerase Reaction. Biochemistry. 1992; 31:1521–1528. [PubMed: 1346570]
12. Zhao Q, Abeygunawardana C, Gittis AG, Mildvan AS. Hydrogen bonding at the active site of Δ^5-3-ketosteroid isomerase. Biochemistry. 1997; 36:14616–14626. [PubMed: 9398180]

13. Mildvan AS, Massiah MA, Harris TK, Marks GT, Harrison DHT, Viragh C, Reddy PM, Kovach IM. Short, strong hydrogen bonds on enzymes: NMR and mechanistic studies. J Mol Struct. 2002; 615:163–175.
14. Frey PA. Strong Hydrogen Bonding in Molecules and Enzymatic Complexes. Magn Reson Chem. 2001; 39:S190–S198.
15. Hawkinson DC, Eames TCM, Pollack RM. Energetics of 3-oxo-Δ^5-steroid isomerase: Source of the catalytic power of the enzyme. Biochemistry. 1991; 30:10849–10858. [PubMed: 1932007]
16. Schwans JP, Kraut DA, Herschlag D. Determining the catalytic role of remote substrate binding interactions in ketosteroid isomerase. Proc Natl Acad Sci USA. 2009; 106:14271–14275. [PubMed: 19706511]
17. Kim D-H, Nam GH, Jang DS, Choi G, Joo S, Kim J-S, Oh B-H, Choi KY. Roles of Active Site Aromatic Residues in Catalysis by Ketosteroid Isomerase from *Pseudomonas putida* Biotype B. Biochemistry. 1999; 38:13810–13819. [PubMed: 10529226]
18. Xue L, Talalay P, Mildvan AS. Studies of the catalytic mechanism of an active-site mutant (Y14F) of Delta-5-3-ketosteroid isomerase by kinetic deuterium isotope effects. Biochemistry. 1991; 30:10858–10865. [PubMed: 1932008]
19. Rasaiah JC, Garde S, Hummer G. Water in Nonpolar Confinement: From Nanotubes to Proteins and Beyond. Annu Rev Phys Chem. 2008; 59:713–740. [PubMed: 18092942]
20. García AE, Hummer G. Water Penetration and Escape in Proteins. PROTEINS: Structure, Function, and Genetics. 2000; 38:261–272.
21. Ball P. Water as an Active Constituent in Biology. Chem Rev. 2008; 108:74–108. [PubMed: 18095715]
22. Maupin CM, Castillo N, Taraphder S, Tu C, McKenna R, Silverman DN, Voth GA. Chemical rescue of enzymes: Proton transfer in mutants of human carbonic anhydrase II. J Am Chem Soc. 2011; 133:6223–6234. [PubMed: 21452838]
23. Feierberg I, Aqvist J. The catalytic power of ketosteroid isomerase investigated by computer simulation. Biochemistry. 2002; 41:15728–15735. [PubMed: 12501201]
24. Mazumder D, Kahn K, Bruice TC. Computational study of ketosteroid isomerase: Insights from molecular dynamics simulation of enzyme bound substrate and intermediate. J Am Chem Soc. 2003; 125:7553–7561. [PubMed: 12812495]
25. Sigala PA, Kraut DA, Caaveiro JMM, Pybus B, Ruben EA, Ringe D, Petsko GA, Herschlag D. Testing geometrical discrimination within an enzyme active site: Constrained hydrogen bonding in the ketosteroid isomerase oxyanion hole. J Am Chem Soc. 2008; 130:13696–13708. [PubMed: 18808119]
26. Fafarman AT, Sigala PA, Herschlag D, Boxer SG. Decomposition of Vibrational Shifts of Nitriles into Electrostatic and Hydrogen-Bonding Effects. J Am Chem Soc. 2010; 132:12811–12813. [PubMed: 20806897]
27. Desmond Molecular Dynamics System. 2.2. D.E. Shaw Research; New York: 2008.
28. Nam GH, Jang DS, Cha S-S, Lee T-H, Kim D-H, Hong BH, Yun YS, Oh B-H, Choi KY. Maintenance of alpha-helical structures by phenyl rings in the active-site tyrosine triad contributes to catalysis and stability of ketosteroid isomerase from Pseudomonas putida biotype b. Biochemistry. 2001; 40:13529–13537. [PubMed: 11695900]
29. Xiang, JZ.; Honig, B. JACKAL: A Protein Structure Modeling Package. Columbia University & Howard Hughes Medical Institute; New York: 2002.
30. Gordon JC, Myers JB, Folta T, Shoja V, Heath LS, Onufriev A. H++: a server for estimating pK_as and adding missing hydrogens to macromolecules. Nucleic Acids Res. 2005; 33:W368–W371. [PubMed: 15980491]
31. Jorgensen WL, Chandrasekhar J, Madura JD, Impey RW, Klein ML. Comparison of Simple Potential Functions for Simulating Liquid Water. J Chem Phys. 1983; 79:926–935.
32. Maestro. 9.0. Schrodinger, LLC; New York: 2009.
33. Hornak V, Abel R, Okur A, Strockbine B, Roitberg A, Simmerling C. Comparison of Multiple Amber Force Fields and Development of Improved Protein Backbone Parameters. Proteins: Structure, Function, and Bioinformatics. 2006; 65:712–725.

34. Cornell WD, Cieplak P, Bayly CI, Gould IR, Merz KM Jr, Ferguson DM, Spellmeyer DC, Fox T, Caldwell JW, Kollman PA. A second generation force field for the simulation of proteins, nucleic acids, and organic molecules. J Am Chem Soc. 1995; 117:5179–5197.
35. Bayly CI, Cieplak P, Cornell WD, Kollman P. A well-behaved electrostatic potential based method using charge restraints for deriving atomic charges: The RESP model. J Phys Chem. 1993; 97:10269–10280.
36. Frisch, MJ.; Trucks, GW.; Schlegel, HB.; Scuseria, GE.; Robb, MA.; Cheeseman, JR.; Montgomery, JA., Jr; Vreven, T.; Kudin, KN.; Burant, JC.; Millam, JM.; Iyengar, SS.; Tomasi, J.; Barone, V.; Mennucci, B.; Cossi, M.; Scalmani, G.; Rega, N.; Petersson, GA.; Nakatsuji, H.; Hada, M.; Ehara, M.; Toyota, K.; Fukuda, R.; Hasegawa, J.; Ishida, M.; Nakajima, T.; Honda, Y.; Kitao, O.; Nakai, H.; Klene, M.; Li, X.; Knox, JE.; Hratchian, HP.; Cross, JB.; Adamo, C.; Jaramillo, J.; Gomperts, R.; Stratmann, RE.; Yazyev, O.; Austin, AJ.; Cammi, R.; Pomelli, C.; Ochterski, JW.; Ayala, PY.; Morokuma, K.; Voth, GA.; Salvador, P.; Dannenberg, JJ.; Zakrzewski, VG.; Dapprich, S.; Daniels, AD.; Strain, MC.; Farkas, O.; Malick, DK.; Rabuck, AD.; Raghavachari, K.; Foresman, JB.; Ortiz, JV.; Cui, Q.; Baboul, AG.; Clifford, S.; Cioslowski, J.; Stefanov, BB.; Liu, G.; Liashenko, A.; Piskorz, P.; Komaromi, I.; Martin, RL.; Fox, DJ.; Keith, T.; Al-Laham, MA.; Peng, CY.; Nanayakkara, A.; Challacombe, M.; Gill, PMW.; Johnson, B.; Chen, W.; Wong, MW.; Gonzalez, C.; Pople, JA. Gaussian03, revision E01 ed. Gaussian, Inc; Pittsburgh, PA: 2003.
37. Case, DA.; Darden, TA.; Cheatham, TE., III; Simmerling, CL.; Wang, J.; Duke, RE.; Luo, R.; Walker, RC.; Zhang, W.; Merz, KM.; Roberts, B.; Wang, B.; Hayik, S.; Roitberg, A.; Seabra, G.; Kolossvary, IK.; Wong, KF.; Paesani, F.; Vanicek, J.; Liu, J.; Wu, X.; Brozell, SR.; Steinbrecher, T.; Gohlke, H.; Cai, Q.; Ye, X.; Wang, J.; Hsieh, M-J.; Cui, G.; Roe, DR.; Mathews, DH.; Seetin, MG.; Sagui, C.; Babin, V.; Luchko, T.; Gusarov, S.; Kovalenko, A.; Kollman, PA. AMBER. Vol. 11. University of California; San Francisco: 2010.
38. Wang J, Wolf RM, Caldwell JW, Kollman PA, Case DA. Development and testing of a general Amber force field. J Comput Chem. 2004; 25:1157–1174. [PubMed: 15116359]
39. Darden T, York D, Pedersen L. Particle mesh Ewald - an N.Log(N) method for Ewald sums in large systems. J Chem Phys. 1993; 98:10089–10092.
40. Nose S. A molecular dynamics method for simulations in the canonical ensemble. Mol Phys. 1984; 52:255–268.
41. Hoover WG. Canonical dynamics: Equilibrium phase-space distributions. Physical Review A. 1985; 31:1695–1697. [PubMed: 9895674]
42. Martyna GJ, Tobias DJ, Klein ML. Constant Pressure Molecular Dynamics Algorithms. J Chem Phys. 1994; 101:4177–4189.
43. Brooks, CLI.; Karplus, M.; Pettitt, BM. Proteins: A Theoretical Perspective of Dynamics, Structure, and Thermodynamics. Vol. 71. John Wiley & Sons, Inc; New York: 1988.
44. Meinhold L, Smith JC. Fluctuations and correlations in crystalline protein dynamics: A simulation analysis of staphylococcal nuclease. Biophys J. 2005; 88:2554–2563. [PubMed: 15681654]
45. Luzar A, Chandler D. Structure and Hydrogen Bond Dynamics of Water-Dimethyl Sulfoxide Mixtures by Computer Simultaions. J Chem Phys. 1993; 98:8160–8173.
46. Čuma M, Schmitt UW, Voth GA. A Multi-State Empirical Valence Bond Model for Weak Acid Dissociation in Aqueous Solution. J Phys Chem A. 2001; 105:2814–2823.
47. Guillot B. A Reappraisal of What We Have Learnt During Three Decades of Computer Simulations on Water. J Mol Liq. 2002; 101:219–260.
48. Warshel A, Sharma PK, Chu ZT, Aqvist J. Electrostatic contributions to binding of transition state analogues can be very different from the corresponding contributions to catalysis: Phenolates binding to the oxyanion hole of ketosteroid isomerase. Biochemistry. 2007; 46:1466–1476. [PubMed: 17279612]
49. Kamerlin SCL, Sharma PK, Chu ZT, Warshel A. Ketosteroid isomerase provides further support for the idea that enzymes work by electrostatic preorganization. Proc Natl Acad Sci USA. 2010; 107:4075–4080. [PubMed: 20150513]
50. Chakravorty DK, Soudackov AV, Hammes-Schiffer S. Hybrid quantum/classical molecular dynamics simulations of the proton transfer reactions catalyzed by ketosteroid isomerase: Analysis

of hydrogen bonding, conformational motions, and electrostatics. Biochemistry. 2009; 48:10608–10619. [PubMed: 19799395]

51. Chakravorty DK, Hammes-Schiffer S. Impact of mutation on proton transfer reactions in ketosteroid isomerase: Insights from molecular dynamics simulations. J Am Chem Soc. 2010; 132:7549–7555. [PubMed: 20450180]
52. QSite. 5.5. Schrodinger, LLC; New York: 2009.
53. Hanoian P, Sigala PA, Herschlag D, Hammes-Schiffer S. Hydrogen Bonding in the Active Site of Ketosteroid Isomerase: Electronic Inductive Effects and Hydrogen Bond Coupling. Biochemistry. 2010; 49:10339–10348. [PubMed: 21049962]
54. Jorgensen WL, Maxwell DS, Tirado-Rives J. Development and testing of the OPLS all-atom force field on conformational energetics and properties of organic liquids. J Am Chem Soc. 1996; 118:11225–11236.
55. Cao Y, Beachy MD, Braden DA, Morrill L, Ringnalda MN, Friesner RA. Nuclear-magnetic-resonance shielding constants calculated by pseudospectral methods. J Chem Phys. 2005; 122:224116. [PubMed: 15974660]
56. Dunning TH Jr. Gaussian basis sets for use in correlated molecular calculations: 1. The atoms boron through neon and hydrogen. J Chem Phys. 1989; 90:1007–1023.
57. Jeffrey J, Yeon Y. The correlation between hydrogen-bond lengths and proton chemical shifts in crystals. Acta Crystallography B. 1986; 42:410–413.

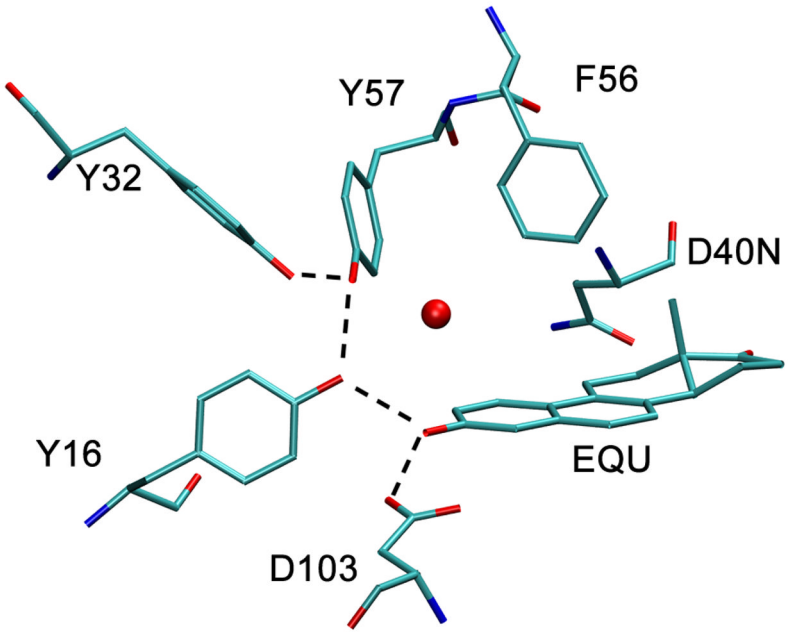

Figure 1.
The pKSI D40N active site with bound EQU from the 1OGX crystal structure, with the active site water molecule identified in the 3FZW crystal structure (pKSI D40N/D103N with bound EQU) shown as a red sphere. This water molecule was added by superimposition of the heavy atoms of EQU in both structures. The hydrogen-bonding network with O–O distances < 2.8 Å is depicted with dotted lines.

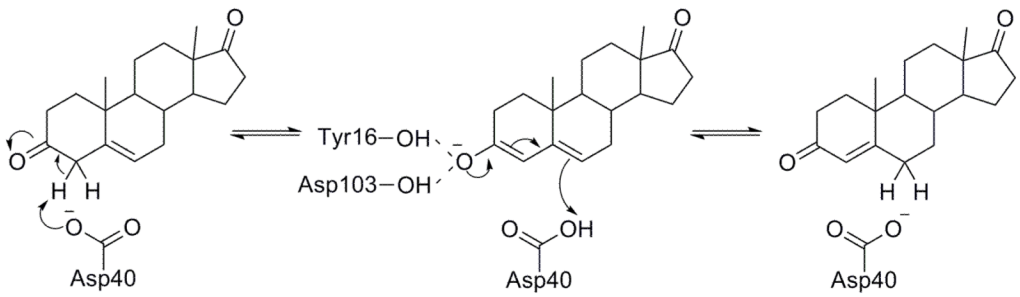

Figure 2.
The mechanism of the isomerization reaction of the 5-AND substrate catalyzed by pKSI. The hydrogen bond donors Tyr16 and Asp103 are shown for the dienolate intermediate state.

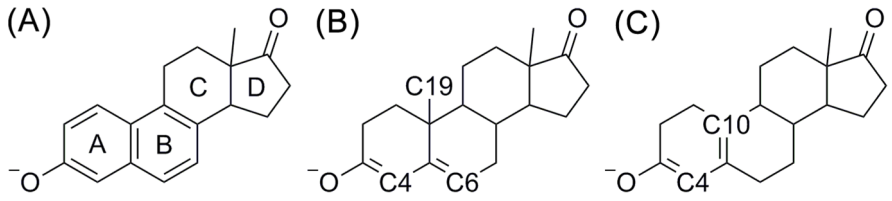

Figure 3.

The ligands used in the MD simulations: (A) equilenin (EQU), (B) the dienolate intermediate form of 5-androstene-3,17-dione (5-AND), and (C) the dienolate intermediate form of 5,10-estrene-3,17-dione (5,10-EST). The proton donor and acceptor carbons of the steroid ligands, the C19 methyl group of 5-AND, and the rings of EQU are labeled.

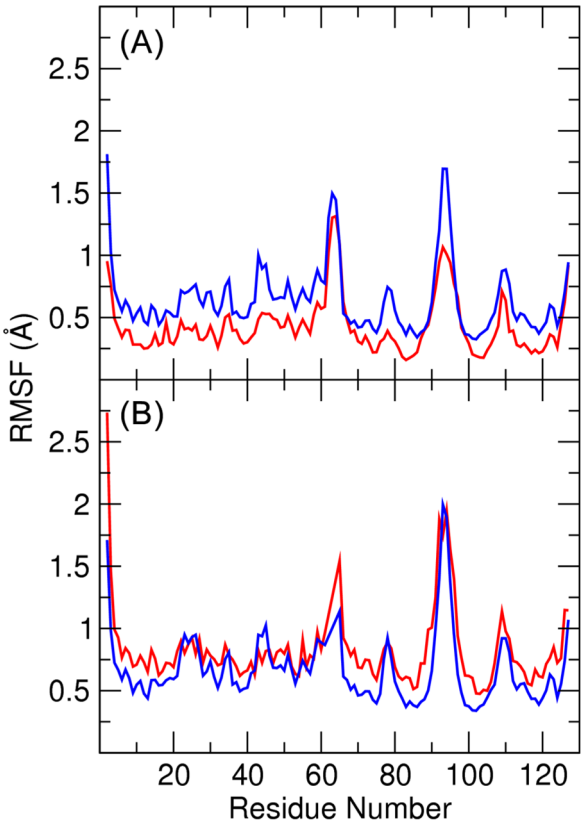

Figure 4.
Comparison of the root mean squared fluctuations of C_α atoms calculated from MD simulations (blue) and from X-ray crystallographic B-factors (red) for (A) the pKSI D40N mutant with bound EQU (PDB: 1OGX) and (B) the pKSI Y16S/D40N mutant with bound EQU (PDB: 3IPT).

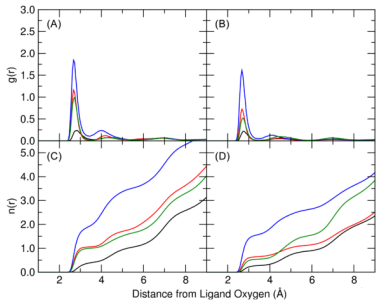

Figure 5.

The radial distribution function $g(r)$ between the ligand oxygen and water oxygens (panels A and B) and the running coordination number $n(r)$ of water oxygens about the ligand oxygen (panels C and D) determined from the 20 ns MD trajectories of pKSI with bound EQU (panels A and C) and with bound 5,10-EST (panels B and D). Data are provided for WT pKSI (black), the Y16F mutant (red,), the Y16S mutant (blue), and the FFF mutant (green). The data shown are averages of data obtained for the active sites of chains A and B and from two independent trajectories.

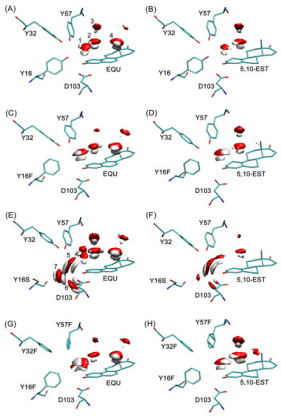

Figure 6.

Representative atomic isodensity surfaces of water oxygen (red) and water hydrogen (white) determined from the 20 ns MD trajectories of four KSI species with two different ligands. Data are shown for WT pKSI (A and B), the Y16F mutant (C and D), the Y16S mutant (E and F), and the FFF mutant (G and H) with bound EQU (A, C, E, and G) and bound 5,10-EST (B, D, F, and H). The average structures of the heavy atoms of active site residues are shown with residue 40 omitted for clarity. An isovalue of three times the water density of the system is plotted in each case.

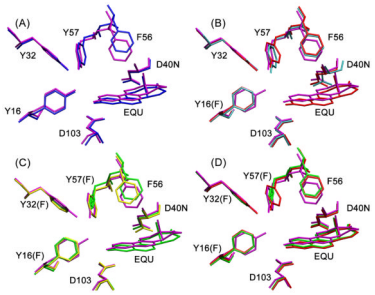

Figure 7.

Comparisons among the average structures from MD trajectories with bound EQU and published crystal structures: (A) the WT MD data (blue) and the WT-EQU crystal structure 1OGX (magenta); (B) the Y16F mutant MD data (red), the WT-EQU crystal structure 1OGX (magenta), and the Y16F-EQU crystal structure 1OHO (cyan); (C) the FFF mutant MD data (green), the WT-EQU crystal structure 1OGX (magenta), and the apo FFF crystal structure 1E97 (yellow); (D) the Y16F mutant MD data (red), the FFF mutant MD data (green), and the WT-EQU crystal structure 1OGX (magenta). Structures were aligned by minimization of the RMSD of the monomer with respect to the backbone C_α atoms resolved in the crystal structure.

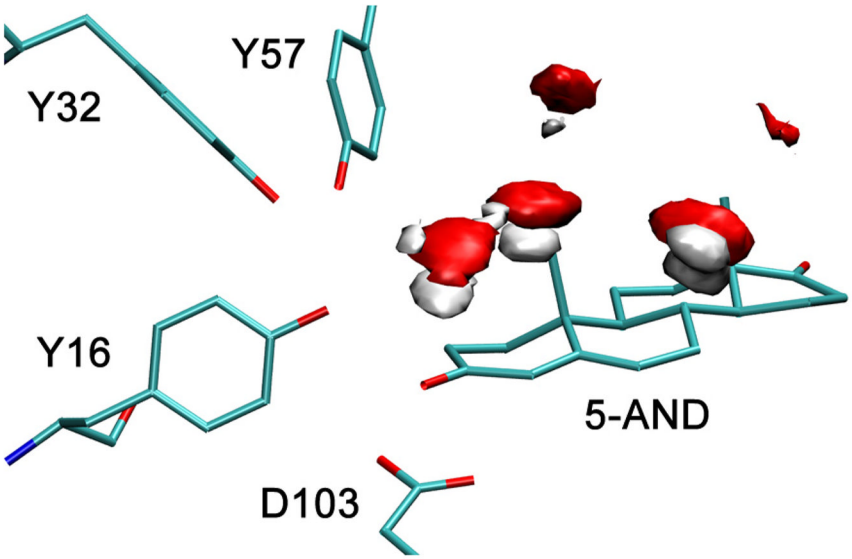

Figure 8.

Replacement of EQU by 5-AND in Figure 6A, which depicts the atomic isodensity surface and the average active site structure determined from a 20 ns MD trajectory of WT pKSI with bound EQU. This figure illustrates the steric clashes between hydrophobic groups in 5-AND and water sites 2 and 4. The position of 5-AND was determined by aligning the average structures determined from two MD trajectories: WT pKSI with bound EQU and WT pKSI with bound 5-AND. This alignment was performed by minimization of the RMSD of the heavy atoms of the active site residues shown (16, 32, 57, and 103).

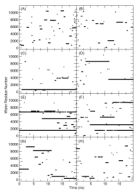

Figure 9.

The (arbitrary) residue number of any water oxygen within 3.5 Å of the ligand oxygen as a function of time for a representative set of 20 ns MD trajectories. Data are shown for WT pKSI (A and B), the Y16F mutant (C and D), the Y16S mutant (E and F), and the FFF mutant (G and H) with bound EQU (A, C, E, and G) and bound 5,10-EST (B, D, F, and H). This figure qualitatively illustrates the exchange rate of water in the active site of each species with bound ligand. Since this figure is intended to depict occupancy of water sites rather than hydrogen bonding, no angular criterion was used.

Table 1

Average number of hydrogen bonds involving the ligand oxygen for each species and each ligand, with standard deviations given in parentheses. These results were obtained by averaging over both active sites and two independent 20 ns MD trajectories for each type of system.

Species	EQU	5,10-EST
WT	2.18 (0.58)	2.04 (0.56)
Y16F	1.85 (0.49)	1.74 (0.51)
Y16S	2.50 (0.71)	2.13 (0.70)
FFF	1.81 (0.44)	1.23 (0.46)

Table 2

Percentage of configurations satisfying the hydrogen bond definition of O–O distance < 3.5 Å and O-H-O angle within 30° of linearity involving the ligand oxygen for each species and each ligand. These results were obtained by averaging over both active sites and two independent 20 ns MD trajectories for each type of system. For water, configurations were distinguished based on the number of simultaneous hydrogen bonds from water to the ligand oxygen. Standard deviations among the data sets are given in parentheses.

	WT		Y16F		Y16S		FFF	
Hydrogen Bond Donor	**EQU**	**5,10-EST**	**EQU**	**5,10-EST**	**EQU**	**5,10-EST**	**EQU**	**5,10-EST**
Tyr16(Ser)	93.2 (0.7)	94.3 (1.8)	NA	NA	0.0	0.0	NA	NA
Asp103	90.3 (1.2)	84.2 (4.7)	95.2 (3.9)	91.7 (4.4)	89.6 (0.1)	81.1 (2.6)	97.5 (0.3)	97.2 (0.5)
Tyr57	4.2 (1.8)	5.1 (6.2)	2.6 (2.1)	34.2 (25.0)	2.6 (5.0)	16.1 (11.7)	NA	NA
$H_2O(1)$	30.4 (8.0)	20.0 (3.7)	76.4 (6.2)	43.4 (24.9)	30.6 (1.8)	41.2 (14.9)	79.9 (3.0)	37.8 (9.9)
$H_2O(2)$	0.0	0.0	5.3 (7.0)	2.5 (4.7)	57.1 (7.7)	30.7 (13.4)	1.8 (1.0)	0.0
$H_2O(3)$	0.0	0.0	0.0	0.0	4.3 (1.7)	0.1 (0.1)	0.0	0.0

Table 3

Hydrogen bonding O–O distances obtained by QM/MM geometry optimization averaged over configurations sampled at intervals of 1 ns from a 20 ns MD trajectory, with standard deviations given in parentheses.

H-bond Distance (Å)	WT	Y16F	Y16S	FFF
Tyr16-EQU	2.52 (0.08)	NA	NA	NA
Asp103-EQU	2.62 (0.06)	2.55 (0.06)	2.57 (0.04)	2.52 (0.04)
Tyr57-Tyr16	2.72 (0.30)	NA	NA	NA
Tyr32-Tyr57	2.85 (0.15)	2.95 (0.51)	2.79 (0.04)	NA
H_2O-EQU	2.86 (0.18)	2.67 (0.08)	2.72 (0.48)	2.72 (0.10)

Table 4

^{1}H NMR chemical shifts of hydrogen-bonded protons from QM/MM geometry optimization averaged over configurations sampled at intervals of 1 ns from a 20 ns MD trajectory, with standard deviations given in parentheses.

^{1}H Chemical Shift (ppm)	WT	Y16F	Y16S	FFF
Tyr16	16.9 (3.0)	NA	NA	NA
Asp103	14.1 (1.2)	15.7 (1.2)	14.9 (0.8)	16.5 (1.1)
Tyr57	11.4 (3.2)	8.0 (0.9)	8.9 (1.0)	NA
Tyr32	8.1 (0.7)	7.6 (0.7)	8.4 (0.5)	NA